Journal of Power Sources 186 (2009) 261–267

Contents lists available at ScienceDirect

Journal of Power Sources

journal homepage: www.elsevier.com/locate/jpowsour

Electrochemical activity and stability of dealloyed Pt–Cu and Pt–Cu–Co electrocatalysts for the oxygen reduction reaction (ORR)

K.C. Neyerlin[a], Ratndeep Srivastava[a], Chengfei Yu[a], Peter Strasser[a,b,*]

[a] Department of Chemical & Biomolecular Engineering, University of Houston, Houston, TX 77204, United States
[b] Institut fuer Chemie, Technische Universitaet Berlin, 10623 Berlin, Germany

ARTICLE INFO

Article history:
Received 23 August 2008
Received in revised form 5 October 2008
Accepted 7 October 2008
Available online 25 October 2008

Keywords:
PEM fuel cell
Dealloyed Pt electrocatalysts
Oxygen reduction reaction
Alloy nanoparticles
Pt Cu Co ternary alloys
Electrocatalysis

ABSTRACT

A comparative study of the electrochemical stability of $Pt_{25}Cu_{75}$ and $Pt_{20}Cu_{20}Co_{60}$ alloy nanoparticle electrocatalysts in liquid electrolyte half-cell environment was conducted. The aforementioned catalysts were shown to possess improved resistance to electrochemical surface area (ECSA) loss during voltage cycling relative to commercially available pure Pt electrocatalysts. The difference in ECSA loss was attributed to their initial mean particle size, which varied depending on the temperature at which the alloy catalysts were prepared (e.g. 600, 800 and 950 °C). Higher preparation temperatures resulted in larger particles and lead to lower ECSA loss. Liquid electrolyte environment short-term durability testing (5000 voltages cycles) revealed the addition of cobalt to be beneficial as ternary compositions exhibited stability advantages over binary catalysts.

Oxygen reduction reaction (ORR) activity and catalyst stability tests were then performed for both $Pt_{25}Cu_{75}$ and $Pt_{20}Cu_{20}Co_{60}$ alloy catalysts in membrane electrode assemblies (MEA). ORR activity data, taken both prior to and at the conclusion of 30,000 voltage cycles from 0.5 to 1.0 V vs. reversible hydrogen electrode (RHE), revealed that both $Pt_{25}Cu_{75}$ and $Pt_{20}Cu_{20}Co_{60}$ were able to retain both their mass and Pt surface area-based activity advantage relative to Pt/C [R. Srivastava, P. Mani, N. Hahn, P. Strasser, Angew. Chem. Int. Ed. 46 (2007), 8988; P. Mani, R. Srivastava, P. Strasser, J. Phys. Chem. C 112 (2008), 2770; S. Koh, P. Strasser, J. Am. Chem. Soc. 129 (2007), 12624]. Further analysis revealed that the Pt surface area-based activity, measured at 0.9 V vs. RHE, of commercially available Pt catalysts, as well as that for both $Pt_{25}Cu_{75}$ and $Pt_{20}Cu_{20}Co_{60}$ increased on the order of tens of $\mu A\,cm_{Pt}^{-2}$ per 1000 voltage cycles. This increase in specific activity combined with a reduced ECSA loss resulted in a negligible change for the Pt mass-based activity of $Pt_{25}Cu_{75}$ alloys annealed at 950 °C.

1. Introduction

Alloy catalysts that have been voltammetrically dealloyed, producing Pt rich surfaces and alloy rich cores, such as dealloyed $Pt_{25}Cu_{75}$ and $Pt_{20}Cu_{20}Co_{60}$ nanoparticles, have been shown to exhibit significantly improved activity for oxygen reduction in acidic media due to a reduced Pt–Pt atomic distance [1–3]. However, as with most cathode catalysts promoted for use in proton exchange membrane fuel cells (PEMFC), questions remain regarding their resistance to electrochemical surface area degradation and long-term oxygen reduction activity stability. Several groups have reported that voltage cycling, either in an electrochemical half-cell, e.g. [4,5] or full membrane electrode assembly (MEA) configuration, e.g. [6–10] increases catalyst particle size, reducing available electrochemical surface area (ECSA in $m^2\,g_{cat}^{-1}$) and therefore should increase voltage loss (due to an increase in oxygen reduction overpotential). Furthermore, Pt dissolution or particle growth have been shown to be a function of potential [11,12], fuel cell operating temperature [7,8], relative humidity [7], and the presence of water [13–16], making it difficult to theoretically predict the resulting ECSA change over time in various Pt alloy systems. For Pt alloy nanoparticle catalysts, the issue of stability has often been convoluted due to the cross-comparison of alloys with various preparation conditions or particle size. Consequently, in previous studies it was not clear whether stability advantages of Pt alloy nanoparticles stem from alloy metal components or from variations in the synthesis process.

The objective of this contribution is to address the effects of preparation conditions, specifically annealing temperature and initial catalyst particle size, on the stability of pure Pt versus Pt alloy nanoparticles. To normalize for both annealing temperature and particle size effects, commercially available Pt catalysts, Pt sup-

* Corresponding author at: Department of Chemical & Biomolecular Engineering, University of Houston, S222, Engineering BLDG 1, 4800, Calhoon Rd., Houston, TX 77204, USA. Tel.: +1 713 743 4300.
E-mail address: pstrasser@uh.edu (P. Strasser).

0378-7753/$ – see front matter © 2008 Elsevier B.V. All rights reserved.
doi:10.1016/j.jpowsour.2008.10.062

ported on high surface area carbon (Pt/HSC) and Pt supported on Vulcan XC72 (Pt/Vu), were subjected to preparation conditions identical to that of alloys prepared at 800 °C (see Section 2 for further details). These "heat treated" catalysts, denoted as HT-Pt/HSC and HT-Pt/Vu, were shown to have a lower normalized ECSA loss then their "as received" counterparts (i.e. commercially available catalysts used as received). After comparing N-ECSA data for 5000 voltages cycles from 0.5 to 1.0 V vs. RHE in liquid electrolyte, we then moved to MEA tests of ECSA stability by subjecting Pt/HSC, Pt/Vu, $Pt_{25}Cu_{75}$ and $Pt_{20}Cu_{20}Co_{60}$ catalysts to 30,000 voltages cycles from 0.5 to 1.0 V vs. RHE. In addition to ECSA stability, in order to determine the activity stability of the catalysts, ORR activity data, compared at 0.9 V vs. RHE, was taken both prior to and at the conclusion of 30,000 voltage cycles.

2. Experimental

2.1. Catalyst preparation

$Pt_{25}Cu_{75}$ and $Pt_{20}Cu_{20}Co_{60}$ alloys were prepared by an impregnation/freeze drying route followed by annealing. Preparation started with impregnation and sonication of a commercial high surface area carbon 28.1 wt% Pt catalyst supplied by Tanaka Kikinzoku International, Inc. (Pt/HSC) with aqueous metal–salt solutions ($Cu(NO_3)_2$ or $Co(NO_3)_2$—Sigma–Aldrich, Inc.). Once this slurry was sonicated, the impregnated catalysts were then frozen in liquid N_2 and subsequently freeze-dried under a moderate vacuum (0.055 mbar). Reduction and alloying/annealing of Pt with either Cu or Co on the carbon support was thermally driven under a reductive H_2 atmosphere (6% H_2, balance Ar) using a Lindberg/Blue tube furnace at temperatures of either 600, 800, or 950 °C for 7 h. Commercially available Pt/HSC and Pt/Vulcan XC72 (referred to as Pt/Vu henceforth, supplied by BASF, E-tek Corp.) were also exposed to an H_2 atmosphere at 800 °C to aid in comparisons of ECSA loss. (*Note*: the abbreviation HT denotes such catalysts, e.g. HT-Pt/HSC, HT-Pt/Vu.)

2.2. X-ray diffraction measurements

Laboratory-source XRD (Siemens D5000 y/2y Diffractometer) was used to characterize the electrocatalysts structurally. The diffractrometer is equipped with a Braun Position Sensitive Detector (PSD) with an angular range of 81. The Cu Kα source operates at a potential of 35 kV and current of 30 mA. 2 θ diffraction angles ranged from 20 to 70°, scanned with step size of 0.02° per step and holding time of 10–30 s per step. Advanced X-ray Solution (X-ray commander, Bruker AXS) software was used to control the diffractometer from a desktop computer. The XRD sample holder was a custom-made 3 cm × 3 cm plexiglass with a 1 cm width × 2 cm length × 1 mm depth well in the center that hold the powder catalyst samples. The catalyst powder was poured into the well and carefully flattened to form a smooth surface, flushed with the surface of the plexiglass. All XRD diffraction patterns were analyzed using Jade (MDI). Each peak profile of each reflection was obtained by a non-linear least square fit of the Kα2 and background corrected data. Instrumental broadening was determined using an alumina standard under identical measurement conditions. Particle sizes were estimated using the observed line broadening and Scherrer equation at several fundamental reflections.

2.3. Liquid electrolyte durability testing

Liquid electrolyte tests were conducted in a 16 chamber electrochemical array described elsewhere [17]. In short, each individual compartment, machined from a piece of polyvinylidene fluoride (PVDF), contained its own counter (Pt wire, Alfa Aesar), reference (Ag/AgCl from Bioanalytical Systems) and working electrodes (10 mm diameter glassy carbon, 0.7584 cm^2 from Hochtemperatur-Werkstoffe GmbH, Germany). Inks were prepared in a manner nearly identical to that for RDE experiments [3]. 10 mg of the desired catalyst was combined with 7.96 mL of DI water, 2 mL of isopropanol and 40 μL of 5 wt% Nafion solution (Aldrich). The ink was then horn sonicated in a surrounding water bath for 15 min. After sonication, 39.1 μL of the ink was deposited onto each of the glassy carbon (GC) electrodes resulting in Pt loadings of 14 $\mu g_{Pt}\ cm^{-2}_{electrode}$ for pure Pt/C catalysts [18,19] and a range of 10–11 $\mu g_{Pt}\ cm^{-2}_{electrode}$ for the alloys. The entire array was then placed into a N_2 atmosphere and left to dry for about 1 h. The chambers were then filled with 0.1 M $HClO_4$ and bubbled with N_2 for 15 min, gas flow was then switched to a blanketing flow, similar to that of a conventional RDE set up. 5000 voltage cycles were performed from 0.5 to 1.0 V vs. RHE at room temperature (about 25 °C) and a rate of 100 mV s^{-1}. CVs were taken periodically throughout the testing procedure from 0.05 to 1.2 V vs. RHE at a sweep rate of 10 mV s^{-1}, 2 mV log rate. A value of 210 $\mu C\ cm^{-2}_{Pt}$ was used to determine the surface area of Pt available from hydrogen adsorption [20].

2.4. MEA durability testing

Procedures for MEA preparation and electrochemical dealloying are described in detail elsewhere [1,2]. In short, catalyst inks were spray coated directly onto Nafion NRE212 membranes (resulting in cathode loadings of about 0.2 $mg_{Pt}\ cm^{-2}$), once dry the 10 cm^2 MEA was assembled in a fuel cell between two SGL 10BC diffusion media. The $Pt_{25}Cu_{75}$ and $Pt_{20}Cu_{20}Co_{60}$ catalysts were then electrochemically dealloyed via voltage cycling (for detailed procedure see Mani et al. [2] or Srivastava et al. [1]). All MEAs were then exposed to a break-in period at 80 °C, 100% relative humidity (RH), with gas partial pressures of 101.3 and stoics of 2 and 9.5 for neat H_2 and O_2 respectively, holding at 0.6 V vs. RHE for 24 h. After this break-in period, voltage cycling commenced from 0.5 to 1.0 V at 100 mV s^{-1} with H_2/N_2 flows of 160 ml min^{-1} and a cell temperature and RH of 80 °C and 100%. CVs were taken periodically throughout the testing procedure from 0.05 to 1.2 V vs. RHE at a sweep rate of 20 mV s^{-1} with a cell temperature of 30 °C and a humidifier temperature of 50 °C. A value of 210 $\mu C\ cm^{-2}_{Pt}$ was used to determine the surface area of Pt available from hydrogen adsorption. Polarization curves were also collected prior to and immediately after 30,000 voltage cycles to assess ORR activity. Polarization curves were taken at 80 °C, 100% RH, with gas partial pressures of 101.3 kPa_{abs} and stoics of 2 and 9.5 for neat H_2 and O_2, respectively. Presented data has been corrected for both hydrogen crossover as well as cell electronic and protonic resistance, which was determined by taking the real resistance at zero imaginary impedance from AC impedance spectroscopy.

3. Results and discussion

3.1. Pt and Pt alloy stability measurements in liquid electrolyte

To make accurate comparisons regarding Pt ECSA loss between commercially available Pt/HSC and Pt/Vu and the $Pt_{25}Cu_{75}$ and $Pt_{20}Cu_{20}Co_{60}$ alloys presented here, Pt/HSC and Pt/Vu were subjected to 800 °C for 7 h (denoted with HT). This universal pretreatment helped to eliminate the otherwise large discrepancies in particle size, stemming from the plethora of temperatures at which the alloy catalysts can be prepared. According to anomalous X-ray scattering measurements, the various high temperature reduction

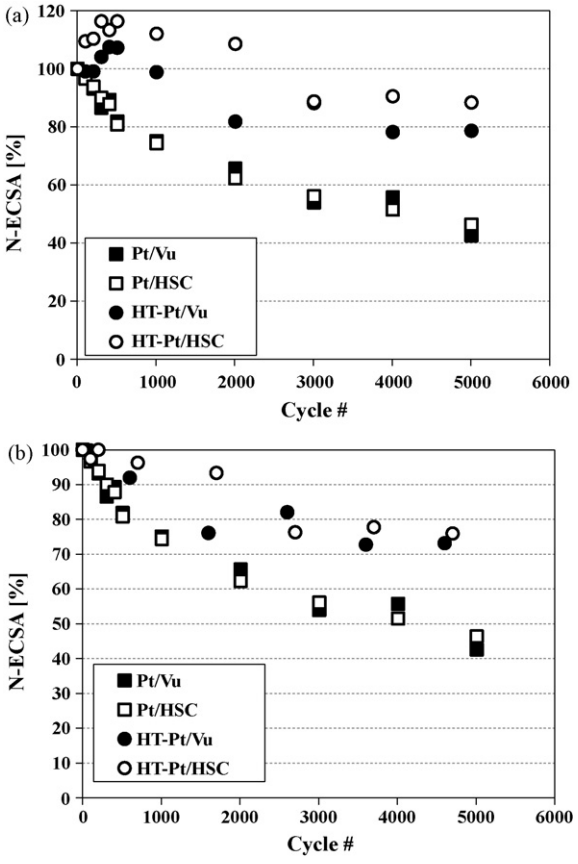

Fig. 1. (a) Normalized ECSA loss due to voltage cycling from 0.5 to 1.0 V vs. RHE for commercially available Pt/Vu and Pt/HSC as well as for commercially available catalysts exposed to 6% H_2 (balance Ar) for 7 h at 800 °C (HT-Pt/Vu and HT-Pt/HSC). (b) Normalized ECSA loss relative to maximum ECSA due to voltage cycling from 0.5 to 1.0 V vs. RHE for commercially available Pt/Vu and Pt/HSC as well as for commercially available catalysts exposed to 6% H_2 (balance Ar) for 7 h at 800 °C (HT-Pt/Vu and HT-Pt/HSC).

procedures have been shown to result in mean particle sizes of 2.95, 3.51, and 4.65 nm for 600, 800, and 950 °C, respectively [21] as compared to the mean initial particle size of 1.9 nm for commercially available Pt/C catalysts [7].

Fig. 1a displays the normalized ECSA remaining with respect to cycle number for Pt/Vu, Pt/HSC, HT-Pt/Vu and HT-Pt/HSC exposed to voltage cycles from 0.5 to 1.0 V vs. RHE at 100 mV s^{-1}. (*Note*: N-ECSA = ECSA at cycle *x*/ECSA initial × 100.) It should be noted that the results for both as received Pt/Vu and Pt/HSC correlate with those of Borup et al. where it was found that only 60% of the initial ECSA remains after 1500 voltage cycles from 0.1 to 1.0 V for such as received catalysts [7]. What becomes evident quickly in Fig. 1a is that the two catalysts have a significant disparity in "break-in time" (i.e. the time it takes the catalyst to obtain its maximum ECSA). While the as received Pt/C catalysts obtain maximum ECSA after only a few cycles, it takes hundreds of cycles for the HT samples to do the same. Whether due to additional time needed to sufficiently wet the HT catalyst or due to surface rearrangement of Pt atoms to more stable conformations during the heat treatment process, it is obvious that the HT process clearly effects the "break-in time". From this point to help draw more accurate conclusions regarding trends in ECSA, plots and tables will discuss both ECSA and N-ECSA with respect to each catalysts maximum ECSA (be it after 100 cycles or several hundred cycles). Fig. 1b illustrates the remaining N-ECSA (from maximum ECSA) for commercially available Pt/Vu, Pt/HSC as well as those for HT-Pt/Vu and HT-Pt/HSC. From Fig. 1b it can be

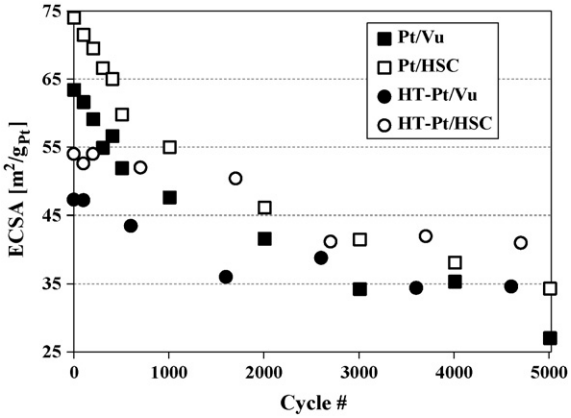

Fig. 2. ECSA over the course of 5000 voltages cycles from 0.5 to 1.0 V vs. RHE for commercially available Pt/Vu and Pt/HSC as well as for commercially available catalysts exposed to 6% H_2 (balance Ar) for 7 h at 800 °C (HT-Pt/Vu and HT-Pt/HSC).

surmised that exposure to high temperatures has a significant effect on ECSA loss as on average both HT samples retain 75% of their initial area, compared to only around 45% for the commercially available Pt/HSC and Pt/Vu. In addition the near perfect overlap of N-ECSA trends for both HT and "as received" samples with respect to their N-ECSA indicates that ECSA loss due to voltage cycling from 0.5 to 1.0 V is dictated by particle coarsening and possible dissolution of Pt (and hence the pretreatment or fabrication technique of the catalyst) and not by the carbon support. Thus, it becomes apparent that one should compare durability on catalysts prepared in the same manner, be it chemical or thermal reduction, in order to draw accurate conclusions on the effect various alloy compositions may have on Pt ECSA degradation.

In the preceding paragraphs stability was evaluated on a relative basis, Fig. 2 shows the ECSA loss in absolute terms. Although N-ECSA losses are reduced in HT samples in Fig. 1b, after 5000 voltages cycles there is only a slight ECSA advantage in absolute terms (about 7 $m^2\ g_{Pt}^{-1}$) for HT samples. Using a simplified kinetic model describing the $E_{iR\text{-free}}$ vs. log *i* Tafel relation between measured geometric current density (*i*) and cell voltage ($E_{iR\text{-free}}$) [22]

$$E_{iR\text{-free}} = 0.9 - \frac{2.303RT}{\alpha_c F} \log\left[\frac{i}{10 L_{ca}\, ECSA\, i_s^{*(0.9\,V)}}\right] \quad (1)$$

this small difference in ECSA amounts to a mere 8 mV of voltage difference between the HT and as received Pt/C catalysts. This assumes a cell temperature $T = 80$ °C, H_2 and O_2 gas partial pressures of 101.3 kPa, a typical Pt specific activity at 0.9 V ($i_s^{*(0.9V)}$) of 250 μA cm_{Pt}^{-2}, a Pt cathode loading (L_{ca}) of 0.4 $mg_{Pt}\ cm^{-2}$, and a cathodic transfer coefficient of $\alpha_c = 1$ [22].

Our analysis up to this point evidences a trade-off between absolute ECSA and N-ECSA degradation due to voltage cycling. It also suggests that due to the small difference in cell voltage it is not advisable for Pt catalysts be heated to high temperatures as a means of mitigating ECSA loss. A different situation may arise, however, regarding heat-treated Pt alloy catalysts for which alloy components may cause a substantial difference in durability and activity alike.

Fig. 3a shows N-ECSA for $Pt_{25}Cu_{75}$ and $Pt_{20}Cu_{20}Co_{60}$ alloys reduced/annealed at 600, 800, and 950 °C. The plot illustrates that at every preparation temperature $Pt_{25}Cu_{75}$ alloys (squares) show a much higher N-ECSA loss than $Pt_{20}Cu_{20}Co_{60}$ (triangles). To further demonstrate this point, Fig. 3b shows N-ECSA after 5000 cycles for all six catalysts. In addition to the observation that Co enhances durability for $Pt_{20}Cu_{20}Co_{60}$ alloys relative to $Pt_{25}Cu_{75}$, it becomes inherently clear from Fig. 3b that there exists a positive correlation

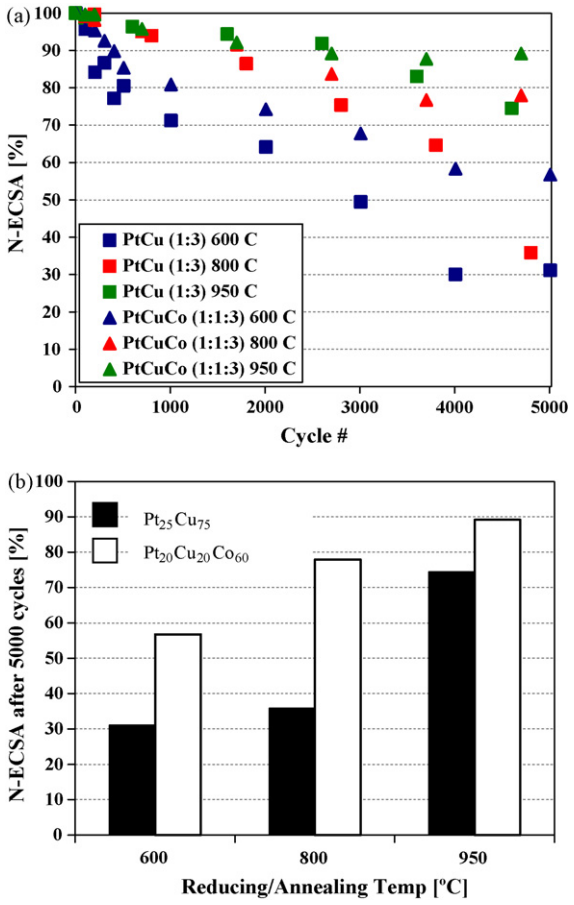

Fig. 3. (a) N-ECSA over the course of 5000 voltages cycles from 0.5 to 1.0 V vs. RHE for PtCu and PtCuCo alloys prepared at various reducing/annealing temperatures. (b) N-ECSA after 5000 voltages cycles from 0.5 to 1.0 V vs. RHE for PtCu and PtCuCo alloys prepared at various reducing/annealing temperatures.

between temperature and N-ECSA retained after voltage cycling, most likely resulting from disparities in initial particle size.

Yu et al. had previously claimed that PtCo alloys had superior resistance to degradation relative to Pt [9], while Zignani et al. concluded that both Pt and PtCo alloys had similar Pt dissolution rates [10]. The caveat here is that in experiments performed by Yu et al. there existed a significant discrepancy between the initial catalyst crystal size for Pt and PtCo, 2.5 and 4.55 nm respectively, due to the various conditions at which the catalysts were prepared (Pt/C catalysts were tested as received, while PtCo/C catalysts were reduced/annealed at 900 °C) [9]. However, for the experiments performed by Zignani et al. both catalysts had initial crystallize sizes of about 5 nm [10]. To aid in the resolution of this discrepancy, Table 1 displays the initial particle sizes for all catalysts tested along with their preparation conditions and remaining N-ECSA after 5000 cycles, while Fig. 4 plots the relationship between initial mean particle size vs. N-ECSA after 5000 voltage cycles. Both Table 1 and Fig. 4 illustrate how an increase in initial particle size directly correlates with an increase in N-ECSA after 5000 cycles. For this reason it is imperative that initial particle size (i.e. preparation conditions) be considered when comparing relationships between metal content and resistance to surface area loss through voltage cycling. Overall, one can see that despite similar initial particle sizes, $Pt_{20}Cu_{20}Co_{60}$ alloys show improved ECSA stability *in liquid electrolyte* for short-term durability testing. Fig.4 further suggests the existence of distinct stability versus particle size relationships for different Pt alloy materials. Knowledge of these relations would predict the required initial particle size in order to achieve a desired catalyst stability.

Table 1
Catalyst composition, particle size, normalized ECSA after cycling and annealing temperature of commerical as-received and heat treated Pt catalysts as well as dealloyed Pt–Cu and Pt–Cu–Co catalysts.

Catalyst	Initial mean particle size [nm]	N-ECSA after 5000 cycles [%]	T [°C]
PtCu (1:3)	2.65	31.2	600
PtCu (1:3)	4.2	35.9	800
PtCu (1:3)	5.4	75.5	950
PtCuCo (1:1:3)	2.4	56.8	600
PtCuCo (1:1:3)	3.2	78	800
PtCuCo (1:1:3)	4.2	89.2	950
Pt/HSC	2.6	46.4	–
HT Pt/HSC	3.2	76	800
Pt/Vu	2.9	42.6	–
HT Pt/Vu	4.8	73.2	800

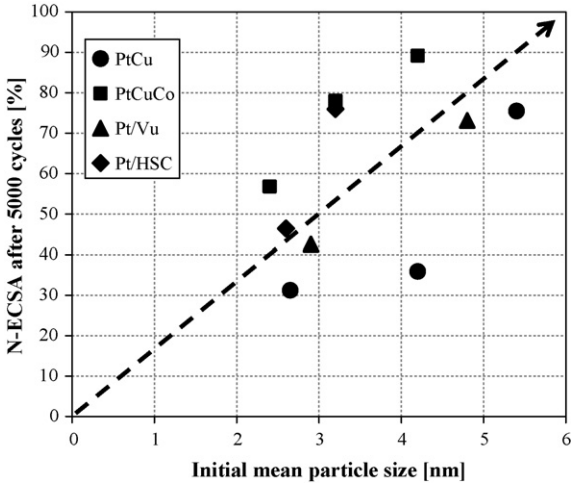

Fig. 4. Initial mean particle size vs. N-ECSA for 5000 voltages cycles from 0.5 to 1.0 V vs. RHE in liquid electrolyte.

3.2. Pt and Pt alloy stability and activity measurements in MEAs

While liquid electrolyte measurements may be more convenient, positive correlations for both modelled [23] and measured

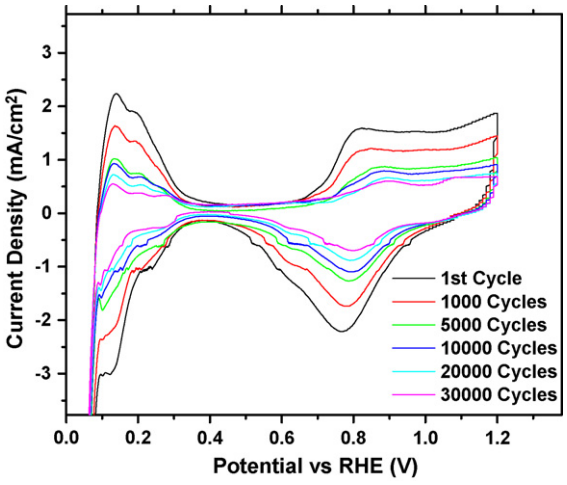

Fig. 5. CVs for a 45 wt% Pt/Vu MEA with a loading of 0.14 mg_{Pt} cm^{-2}. All CVs were taken at a scan rate of 20 mV s^{-1} with a cell temperature of 30 °C, a humidification temp of 50 °C, flow rate of 160 ml min^{-1} for pure H_2 and N_2.

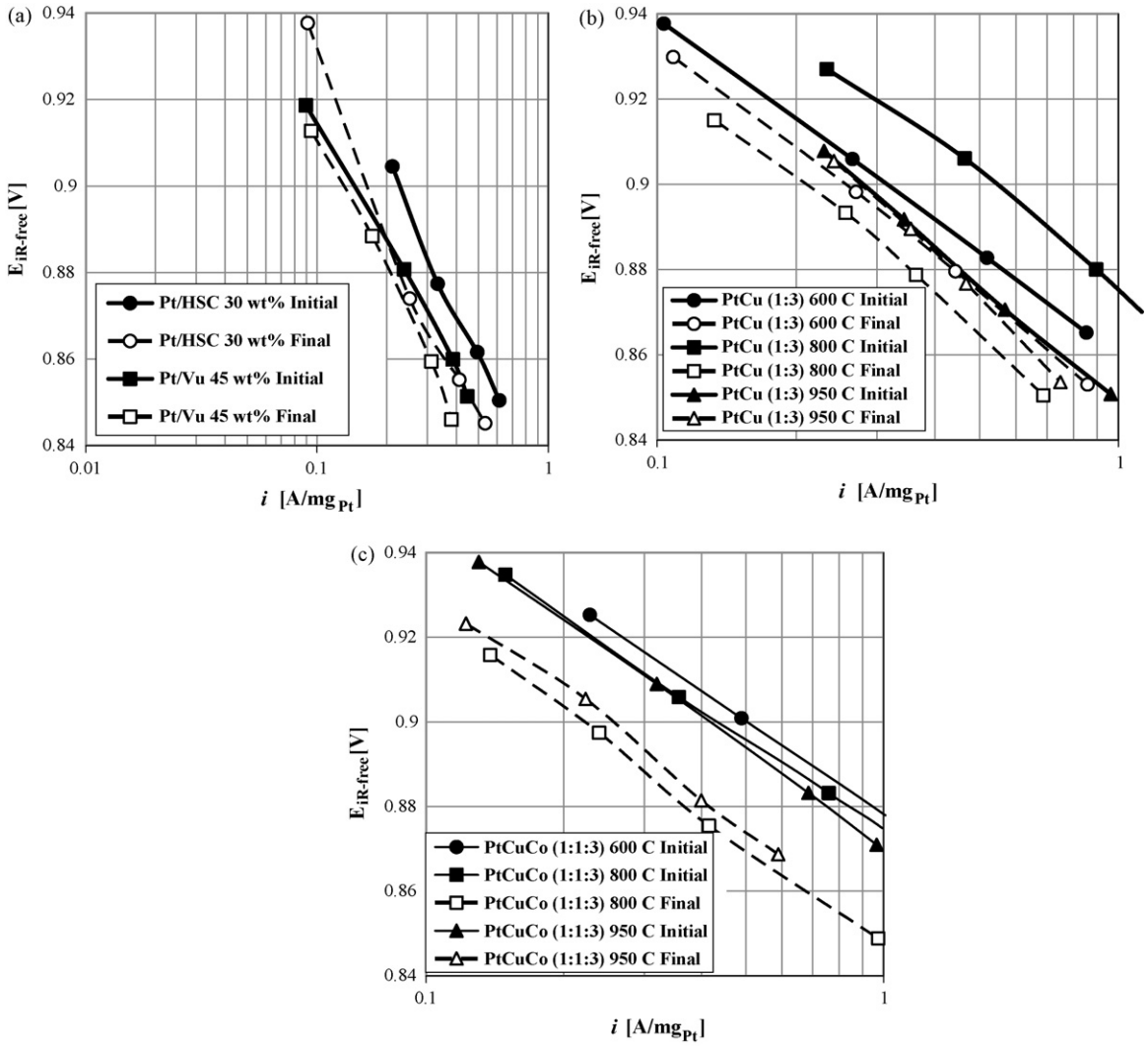

Fig. 6. Ohmic corrected ($E_{iR\text{-free}}$) polarization curves taken at 80 °C, 100% RH, with gas partial pressures of 101.3 kPa_{abs} and stoics of 2 and 9.5 for neat H_2 and O_2, respectively for; (a) Pt/HSC and Pt/Vu, (b) $Pt_{25}Cu_{75}$ and (c) $Pt_{20}Cu_{20}Co_{60}$ catalysts both before ("Initial" solid symbols) and after ("Final" hollow symbols) 30,000 voltage cycles from 0.5 to 1.0 V vs. RHE.

[4] Pt dissolution rates with respect to temperature as well as measurements of increased Pt particle growth rate with respect to both increasing temperature [7,8] and relative humidity [7,24,25], along with the observed acceleration of Pt particle growth in liquid environments [13–16], it is important to measure ECSA stability in fuel cell environments. Fig. 5 displays a series of CVs for an as received 45 wt% Pt/Vu catalyst with a Pt loading of 0.14 $mg_{Pt}\,cm^{-2}$, taken over the course of 30,000 voltage cycles from 0.5 to 1.0 V vs. RHE at 80 °C and 100% RH. While cyclic voltammagrams like Fig. 5 are important tools in assessing catalyst durability, the reduction in ECSA only directly relates to voltage loss for the ORR in instances where catalyst specific activity ($i_s^{*(0.9V)}$) does not vary over the course of such voltage cycles.

Multiple groups have reported variations in specific activity for the ORR over the course of durability cycles [8–10,26], some concluding improvements over time due to catalyst particle size growth [8,9,26], while others have observed a reduction in ORR specific activity in Pt alloys, attributed to the dissolution and redeposition of Pt resulting in a non-alloyed Pt shell [10]. A very detailed review of particle size and other structure-related parameters that effect oxygen reduction is given by Mukerjee and Srinivasan [27]. Here, measurements of mass activity at 0.9 V vs. RHE, $i_m^{(0.9V)}$ (i.e. specific activity ($i_s^{*(0.9V)}$) × ECSA) taken from polarization curves measured at 80 °C, 100% RH, with gas partial pressures of 101.3 kPa_{abs} (for 99.99% pure H_2 and O_2) were performed both after an initial break in period and after 30,000 voltage cycles.

Fig. 6 displays this data for (a) Pt/HSC and Pt/Vu, (b) $Pt_{25}Cu_{75}$ and (c)$Pt_{20}Cu_{20}Co_{60}$ for both before ("Initial" solid symbols) and after ("Final" hollow symbols) 30,000 voltage cycles from 0.5 to 1.0 V vs. RHE. From this polarization data one can see that nearly all of the catalysts have a reduced final mass activity relative to their initial values prior to voltage cycling. Exceptions to this are $Pt_{25}Cu_{75}$ annealed at 600 and 950 °C, where mass activity remains nearly constant despite a reduction in ECSA.

Table 2 summarizes both Pt-mass activities, $i_m^{(0.9V)}$ in $A\,mg_{Pt}^{-1}$, and specific activities, $i_s^{(0.9V)}$ in $\mu A\,cm_{Pt}^{-2}$, for oxygen reduction, as well as N-ECSA retained over the course of these 30,000 voltage cycles. In Table 2 it can be seen that, consistent with the studies presented above in liquid electrolyte, there exists a clear trend where higher annealing temperatures result in higher N-ECSA retained. However, for reasons mentioned above, e.g. Pt dissolution and particle growth dependence on temperature, relative humidity, and the presence of liquid water, it appears that Co does not have a stabilizing effect on Pt dissolution relative to PtCu electrochemi-

Table 2
Catalyst activity parameters in an MEA over the course of 30,000 voltage cycles from 0.5 to 1.0 V vs. RHE at 100 mV s^{-1} and 80 °C, with fully saturated pure H_2 (anode) and N_2 (cathode) feeds of 160 ml min^{-1}.

Catalyst	Annealing temperature [°C]	N-ECSA [%]	$i_m^{0.9V}$ Initial [A mg_{Pt}^{-1}]	$i_m^{0.9V}$ Final [A mg_{Pt}^{-1}]	$i_s^{0.9V}$ Initial [μA cm_{Pt}^{-2}]	$i_s^{0.9V}$ Final [μA cm_{Pt}^{-2}]	$i_s^{0.9V}$ [μA cm_{Pt}^{-2}]/1000 cycles
$Pt_{25}Cu_{75}$	600	35	0.30	0.25	465	1097	21
$Pt_{25}Cu_{75}$	800	55	0.53	0.21	1477	1063	−14
$Pt_{25}Cu_{75}$	950	73	0.32	0.31	944	1250	10
$Pt_{20}Cu_{20}Co_{60}$	600	26	0.49	NA	441	NA	NA
$Pt_{20}Cu_{20}Co_{60}$	800	29	0.42	0.23	894	1677	26
$Pt_{20}Cu_{20}Co_{60}$	950	49	0.42	0.25	1149	1404	9
Pt/HSC 30 wt%	–	23	0.21	0.17	290	787	17
Pt/Vu 45 wt%	–	23	0.16	0.13	279	1056	26

cally dealloyed nanoparticles in MEAs. In addition, any short-term enhancements observed in liquid electrolyte (only 5000 voltage cycles) may become moot over the much longer 30,000 voltage cycles done here for an MEA.

From the 4th column in Table 2, it can be observed that all of the initial mass activities, taken from Fig. 6a–c, for the core–shell Pt alloy nanoparticles are improved relative to Pt/HSC and Pt/Vu, consistent with earlier findings for both $Pt_{25}Cu_{75}$ [2,3] and $Pt_{20}Cu_{20}Co_{60}$ [1]. The 5th column in Table 2 shows that not only are the initial mass activities improved, but both $Pt_{25}Cu_{75}$ and $Pt_{20}Cu_{20}Co_{60}$ are able to maintain their kinetic advantage relative to Pt/HSC and Pt/Vu after 30,000 voltage cycles. To rule out ECSA variations as the underlying cause for these improvements, initial specific activity (μA cm_{Pt}^{-2}) values were tabulated and are displayed in the 6th column of Table 2. From this column one can see that all of the $Pt_{25}Cu_{75}$ and $Pt_{20}Cu_{20}Co_{60}$ catalysts have from 1.5 to 5 times the specific activity of Pt/HSC and Pt/Vu. Specific activity values for the $Pt_{25}Cu_{75}$ and $Pt_{20}Cu_{20}Co_{60}$ catalysts tend to increase with increased annealing temperature, due to increases in alloying and a reduced Pt–Pt atomic distance [2,3,27], Comparing columns 4 and 5 in Table 2 one observes that there are catalysts for which the initial and final mass activity are nearly unchanged (e.g. $Pt_{25}Cu_{75}$ at both 600 and 950 °C), and thus the alloys *final* kinetic advantage relative to the *initial* performance of Pt/HSC and Pt/Vu is maintained. This is due to a combination of improved resistance to ECSA loss as well improvements in specific activity over the course of voltage cycling. In fact, for the majority of tested catalysts the specific activity improves on the order of tens of μA cm_{Pt}^{-2} per 1000 cycles (see last column in Table 2). While these values may vary due to the range of voltages cycled as well as the number of voltage cycles, the average change in specific activity for catalysts tested here, +11 μA cm_{Pt}^{-2} per 1000 cycles, is on the same order of magnitude with values tabulated from plots by Yu et al. [9] +8 and +30 μA cm_{Pt}^{-2} per 1000 cycles for 50 wt% Pt/HSC and 50 wt% PtCo/HSC respectively. This would lead one to conclude that a general trend of improvement in specific activity is on the order of 10 μA cm_{Pt}^{-2} per 1000 cycles.

Previously, it had been observed that alloys of Pt and 3d-transition metals enhanced stability and degradation of Pt via sintering and dissolution of the more oxidizable element [28]. The same research group [28] also demonstrated that *initial* specific activity of both Pt and Pt alloys increased with decreasing ECSA (i.e. increasing particle size, see Fig. 3 in Mukerjee and Srinivasan [27]) allowing one to presume that as catalyst particle size increases over time, as it does in voltage cycling/durability experiments, specific activity will increase. Here, we have demonstrated for the first time that such increases in specific activity for Pt binary and ternary oxygen reduction catalysts can compensate for the loss of ECSA, allowing these dealloyed electrocatalysts to maintain their high rate of oxygen reduction per gram of Pt even after 30,000 durability cycles.

4. Conclusions

$Pt_{25}Cu_{75}$ and $Pt_{20}Cu_{20}Co_{60}$ nanoparticle electrocatalysts were shown to possess improved resistance to ECSA loss during voltage cycling relative to as received commercially available pure Pt electrocatalysts (e.g. Pt/HSC and Pt/Vu). This difference was attributed to both the initial particle size of the catalysts, which is a function of preparation temperature, as well as the elements of which the material was composed. Any short-term ternary catalyst durability improvements observed in liquid electrolyte testing, attributed to the addition of cobalt, disappeared over longer durability tests in MEAs. Measurements of oxygen reduction activity revealed that both $Pt_{25}Cu_{75}$ and $Pt_{20}Cu_{20}Co_{60}$ were able to retain their previously presented kinetic enhancement relative to Pt/C [1–3] after 30,000 voltage cycles in a MEA. More importantly, the study demonstrated that the mass activity of $Pt_{25}Cu_{75}$ catalysts was unchanged over 30,000 voltage cycles in a membrane electrode assembly (MEA) and hence their kinetic advantage relative to the *beginning of life* activity of pure Pt was maintained.

Acknowledgements

The authors would like to thank Greg Bugosh and Rhys Forgie for their diligent work over the summer of 2008. This project was supported by the Department of Energy, Office of Basic Energy Sciences (BES), under grant LAB04-20 via a subcontract with the X-ray Laboratory for Advanced Materials (XLAM) and the Stanford Synchrotron Radiation Laboratory (SSRL). Further support was provided by the National Science Foundation (NSF) under the award #0729722. Acknowledgment is made to the Donors of the American Chemical Society Petroleum Research Fund for partial support of this research (grant #44165). Support by the State of Texas through the Advanced Research Program (ARP) during the 2008–2010 funding period is gratefully acknowledged. Also, partial financial support from Houston Area Research Center (HARC) is gratefully acknowledged. Portions of this research were carried out at the Stanford Synchrotron Radiation Laboratory, a national user facility operated by Stanford University on behalf of the U.S. Department of Energy, Office of Basic Energy Sciences.

References

[1] R. Srivastava, P. Mani, N. Hahn, P. Strasser, Angew. Chem. Int. Ed. 46 (2007), 8988.
[2] P. Mani, R. Srivastava, P. Strasser, J. Phys. Chem. C 112 (2008) 2770.
[3] S. Koh, P. Strasser, J. Am. Chem. Soc. 129 (2007) 12624.
[4] M. Mathias, H. Gasteiger, R. Makharia, S. Kocha, T. Fuller, J. Pisco, Abstr. Pap. Am. Chem. Soc. 228 (2004) U653.
[5] B. Merzougui, S. Swathirajan, J. Electrochem. Soc. 153 (2006) A2220.
[6] C. Grolleau, C. Coutanceau, F. Pierre, J.-M. Leger, Electrochim. Acta 53 (2008) 7157.
[7] R.L. Borup, J.R. Davey, F.H. Garzon, D.L. Wood, M.A. Inbody, J. Power Sources 163 (2006) 76.
[8] W. Bi, T.F. Fuller, J. Electrochem. Soc. 155 (2008) B215.

[9] P. Yu, M. Pemberton, P. Plasse, J. Power Sources 144 (2005) 11.
[10] S.C. Zignani, E. Antolini, E.R. Gonzalez, J. Power Sources 182 (2008) 83.
[11] X. Wang, R. Kumar, D.J. Myers, Electrochem. Solid State Lett. 9 (2006) A225.
[12] V. Komanicky, K.C. Chang, A. Menzel, N.M. Markovic, H. You, X. Wang, D. Myers, J. Electrochem. Soc. 153 (2006) B446.
[13] J.A.S. Bett, K. Kinoshita, P. Stonehart, J. Catal. 41 (1976) 124.
[14] M.S. Wilson, J.A. Valerio, S. Gottesfeld, Electrochim. Acta 40 (1995) 355.
[15] Y.F. Chu, E. Ruckenstein, Surf. Sci. 67 (1977) 517.
[16] J.H. Vleeming, B.F.M. Kuster, G.B. Marin, F. Oudet, P. Courtine, J. Catal. 166 (1997) 148.
[17] K.C. Neyerlin, G. Bugosh, R. Forgie, Z. Liu, P. Strasser, J. Electrochem. Soc., 2008, in press.
[18] U.A. Paulus, T.J. Schmidt, H.A. Gasteiger, R.J. Behm, J. Electrochem. Soc. 495 (2001) 134.
[19] U.A. Paulus, A. Wokaun, G.G. Scherer, T.J. Schmidt, V. Stamenkovic, N.M. Markovic, P.N. Ross, Electrochim. Acta 47 (2002) 3787.
[20] F.C. Nart, W. Vielstich, Normalization of porous active surfaces, in: W. Vielstich, A. Lamm, H.A. Gasteiger (Eds.), Handbook of Fuel Cells: Fundamentals, Technology, and Applications, vol. 2, Wiley, 2003, p. 302, Chapter 21.
[21] C. Yu, S. Koh, J.E. Leisch, M.F. Toney, P. Strasser, Faraday Discuss 140 (2008) 283.
[22] K.C. Neyerlin, W. Gu, J. Jorne, H.A. Gasteiger, J. Electrochem. Soc. 153 (2006) A1955–A1963.
[23] R.M. Darling, J.P. Myers, J. Electrochem. Soc. 150 (2003) A1523.
[24] M.F. Mathias, R. Makharia, H.A. Gasteiger, J.J. Conley, T.J. Fuller, C.J. Gittleman, S.S. Kocha, D.P. Miller, C.K. Mittelsteadt, T. Xie, S.G. Yan, P.T. Yu, Two fuel cell cars in every garage? Electrochem. Soc. Interface (2005) 24.
[25] H. Xu, R. Kunz, J.M. Fenton, Electrochem. Solid State Lett. 10 (2007) B1.
[26] K. Kinoshita, Electrochemical Oxygen Technology, Wiley, New York, 1992.
[27] S. Mukerjee, S. Srinivasan, O_2 reduction and structure-related parameters for supported catalysts, in: W. Vielstich, A. Lamm, H.A. Gasteiger (Eds.), Handbook of Fuel Cells: Fundamentals, Technology, and Applications, vol. 2, Wiley, 2003, p. 503, Chapter 34.
[28] J.S. Buchanan, L. Keck, J. Lee, G.A. Hards, N. Scholey, Proceedings of the First International Fuel Cell Workshop, Tokyo, 1989.